PNAS RESEARCH ARTICLE | PLANT BIOLOGY OPEN ACCESS

A genetically linked pair of NLR immune receptors shows contrasting patterns of evolution

Motoki Shimizu[a,1], Akiko Hirabuchi[a], Yu Sugihara[b], Akira Abe[a], Takumi Takeda[a], Michie Kobayashi[a,c], Yukie Hiraka[a], Eiko Kanzaki[a], Kaori Oikawa[a], Hiromasa Saitoh[a,d], Thorsten Langner[e], Mark J. Banfield[f], Sophien Kamoun[e], and Ryohei Terauchi[a,b,1]

Edited by David Baulcombe, University of Cambridge, Cambridge, United Kingdom; received September 14, 2021; accepted April 19, 2022

Throughout their evolution, plant nucleotide-binding leucine-rich-repeat receptors (NLRs) have acquired widely divergent unconventional integrated domains that enhance their ability to detect pathogen effectors. However, the functional dynamics that drive the evolution of NLRs with integrated domains (NLR-IDs) remain poorly understood. Here, we reconstructed the evolutionary history of an NLR locus prone to unconventional domain integration and experimentally tested hypotheses about the evolution of NLR-IDs. We show that the rice (*Oryza sativa*) NLR Pias recognizes the effector AVR-Pias of the blast fungal pathogen *Magnaporthe oryzae*. Pias consists of a functionally specialized NLR pair, the helper Pias-1 and the sensor Pias-2, that is allelic to the previously characterized Pia pair of NLRs: the helper RGA4 and the sensor RGA5. Remarkably, Pias-2 carries a C-terminal DUF761 domain at a similar position to the heavy metal–associated (HMA) domain of RGA5. Phylogenomic analysis showed that Pias-2/RGA5 sensor NLRs have undergone recurrent genomic recombination within the genus *Oryza*, resulting in up to six sequence-divergent domain integrations. Allelic NLRs with divergent functions have been maintained transspecies in different *Oryza* lineages to detect sequence-divergent pathogen effectors. By contrast, Pias-1 has retained its NLR helper activity throughout evolution and is capable of functioning together with the divergent sensor-NLR RGA5 to respond to AVR-Pia. These results suggest that opposite selective forces have driven the evolution of paired NLRs: highly dynamic domain integration events maintained by balancing selection for sensor NLRs, in sharp contrast to purifying selection and functional conservation of immune signaling for helper NLRs.

nucleotide-binding leucine-rich-repeat receptors (NLRs) | paired NLR | integrated domains | evolution | rice

Significance

Plants have evolved sophisticated defense mechanisms to fend off pathogens. Plant nucleotide-binding leucine-rich-repeat receptor (NLR) proteins play crucial roles in detecting pathogen molecules inside plant cells and mounting defense responses. Here, we identified the *Pias* gene from rice, which encodes the NLR pair Pias-1 "helper" and Pias-2 "sensor." These proteins function together to detect the pathogen molecule AVR-Pias of *Magnaporthe oryzae* and defend against rice blast disease. *Pias* is allelic to the previously reported *Pia* gene. A comparison of Pias/Pia alleles among *Oryza* species showed that the Pias/Pia helper is evolutionarily and functionally conserved, whereas the Pias/Pia sensor shows highly dynamic evolution, with various host domains integrated into similar positions, allowing it to detect a wide variety of pathogen molecules.

Plants are continually attacked by a multitude of microbial pathogens. Pathogens secrete effector molecules to enable the invasion of their hosts (1). To counter this, plants have evolved a surveillance system that detects pathogen effectors inside the plant cell, leading to effector-triggered immunity (ETI) (2). Nucleotide-binding leucine-rich-repeat receptors (NLRs) play pivotal roles in ETI, which frequently leads to hypersensitive response (HR)–mediated cell death (3, 4). NLR genes underwent lineage-specific expansions in most plant genomes (~150 in *Arabidopsis thaliana* and ~500 in rice [*Oryza sativa*]) and are among the most variable genes in plants, pointing to strong selection pressure from pathogens (5, 6). NLR proteins are characterized by a conserved nucleotide-binding (NB) domain and a leucine-rich-repeat (LRR) domain. NLRs are divided into two major groups depending on the type of N-terminal domain: NLRs with the N-terminal coiled-coil (CC) domain are called CNLs (CC-NLRs), and those with the N-terminal Toll-like domain are called TNLs (TIR-NLRs). CNLs are widespread in the plant kingdom. TIRs are grouped into the canonical TIR and TIR2 subclasses. Though TIR2-NB proteins are found in monocot plants, TNLs with canonical TIR domains have been detected in dicot but not in monocot plants (7, 8). Adenosine diphosphate/adenosine triphosphate exchange at the NB domain (9, 10) and oligomerization of NLRs (11–16) trigger ETI signaling. The *Arabidopsis* CNL ZAR1 forms a pentamer "resistosome" complex after binding to a host protein and a pathogen effector. This leads to the protrusion of the N-terminal alpha helix, which perturbs the plasma membrane to trigger the HR (10, 15), a process potentially mediated by Ca^{2+} influx (17). The *Arabidopsis* TNL RPP1 forms a tetramer resistosome upon binding to its cognate effector ATR1, followed by an increase in its NAD^{+}ase activity (11), which triggers cell death (18, 19). These recent breakthroughs have started to reveal the biochemical links between NLR molecular structure and HR induction (20).

NLRs can function as singletons, in pairs, or in networks (4). *Arabidopsis* ZAR1 (10), RPP1 (21), and many other NLRs function as singleton NLRs and recognize avirulence effectors (AVRs) directly or indirectly. Two NLR proteins encoded by

Author contributions: M.S., S.K., and R.T. designed research; M.S., A.H., Y.S., A.A., T.T., M.K., Y.H., E.K., K.O., H.S., S.K., and R.T. performed research; M.S., Y.S., T.L., M.J.B., S.K., and R.T. analyzed data; and M.S., T.L., M.J.B., S.K., and R.T. wrote the paper.

Competing interest statement: S.K. receives funding from the industry on NLR biology.

This article is a PNAS Direct Submission.

[1]To whom correspondence may be addressed. Email: m-shimizu@ibrc.or.jp or terauchi@ibrc.or.jp.

This article contains supporting information online at http://www.pnas.org/lookup/suppl/doi:10.1073/pnas.2116896119/-/DCSupplemental.

Published June 30, 2022.

genetically linked genes function together as paired NLRs. One of the paired NLRs frequently has a noncanonical domain called the integrated domain (ID). IDs are thought to have been derived from other host proteins (8, 22). Examples of paired NLRs include RPS4/RRS1 in *Arabidopsis* (23, 24) and RGA4/RGA5 (25, 26), Pik1/Pik2 (27, 28), and Pii1/Pii2 in rice (29, 30). Multiple NLRs encoded by unlinked genes may function together; these network NLRs (31) include NRC2, NRC3, and NRC4 in Solanaceae plants. When NLRs function as a pair or network, one NLR is involved in the recognition of the AVR effector (the "sensor NLR"), whereas the other plays a role in signaling (the "helper NLR"). Recent studies have expanded our understanding of the genetic architecture of NLR pairs and networks; however, how they function together and how they evolved remain elusive.

A phylogenetic study of 4,184 NLRs in the genomes of 7 Poaceae species including rice, wheat, and other grass species grouped the NLRs into 24 major clades, including 3 clades (MIC1, MIC2, and MIC3) containing the majority of NLRs with IDs (32). NLRs in clade MIC1 (including RGA5) are characterized by a wide variety of IDs integrated into similar positions in the NLR after the LRR domain. The study reported a conserved 43–amino acid motif between the LRR and ID named the CID (conservation and association with IDs) motif. The authors proposed a possible evolutionary mechanism of ID generation and ID shuffling mediated by the CID motif. However, this study examined only a few genomes from each species, with a focus on interspecies diversity within the Poaceae, and provided limited information about the recent diversification of NLRs within a single genus. In addition, experimental validation of the hypotheses underpinning the functional diversity of NLRs with IDs remains limited.

Rice blast disease caused by blast fungus (*Magnaporthe oryzae* [syn. *Pyricularia oryzae*]) is a major disease of rice that threatens world food security (33). The best way to control this disease is to deploy cultivars with resistance (*R*) genes. To date, 40 *R* genes against blast have been reported, and 25 have been cloned, most of which encode NLRs (34, 35). However, the molecular interactions between rice NLRs and blast AVRs are understood for only a small number of cases, including Pita and AVR-Pita (36, 37), Pia and AVR-Pia/AVR1-CO39 (26), Pik and AVR-Pik (28, 38), Pii and AVR-Pii (29, 30, 39), and Pizt and AVR-Pizt (40, 41).

The rice Pia pair, consisting of the NLR helper RGA4 and the NLR sensor RGA5, is one of the most well-characterized NLR pairs (25, 26). Overexpression of *RGA4* in *Nicotiana benthamiana* and rice protoplasts caused HR-like cell death in the respective plant species, suggesting that the helper RGA4 is responsible for HR signaling. RGA4-mediated cell death was suppressed by coexpression of RGA5, indicating that RGA5 negatively regulates RGA4-mediated defense signaling. Finally, coexpression of RGA5, RGA4, and AVR-Pia triggered cell death via the direct binding of AVR-Pia to the heavy metal–associated (HMA) ID of the sensor RGA5 (26). This study, together with a study of the *Arabidopsis* RPS4/RRS1 pair (23, 24), supported a negative regulation model for paired NLRs in which helper NLRs function in HR signaling and sensor NLRs function in the suppression of helper-NLR activity. Upon binding or modification of the sensor-NLR IDs by pathogen AVRs, this suppression is released, allowing HR signaling to proceed. However, a recent study of rice Pikp paired NLRs suggests a helper–sensor cooperation model. Expression of the helper NLR alone did not cause cell death in *N. benthamiana* and coexpression of the helper and sensor was required for triggering effector-dependent HR-like cell death (42).

Here, we describe the rice NLR pair Pias, which recognizes the *M. oryzae* effector AVR-Pias. *Pias* encodes the helper Pias-1 and the sensor Pias-2 and is allelic to the previously characterized *Pia* gene, encoding the NLR pair helper RGA4 and sensor RGA5. Pias-2 carries a C-terminal DUF761 domain at a similar position to the HMA domain of RGA5. We show that the Pias/Pia helper-NLR lineage is evolutionarily and functionally conserved, while its sensor-NLR lineage shows highly dynamic evolution with various host domains integrated into similar positions, possibly allowing it to detect a wide variety of pathogen molecules.

Results

Isolation of Rice *Pias* NLR Genes and the Matching Gene *AVR-Pias* from *M. oryzae*. As part of a large genetic screen to identify novel rice blast resistance genes, we crossed *japonica*-type rice cultivar Hitomebore to 20 different rice cultivars representing the worldwide genetic diversity of rice, resulting in the generation of recombinant inbred lines (RILs) of the F_7 to F_9 generations. We inoculated the parental rice lines with a panel of *M. oryzae* isolates and recorded their resistance or susceptibility to each isolate. Since Hitomebore was susceptible to *M. oryzae* isolate 2012-1 but *indica*-type accession WRC17 [cultivar Keiboba (43)] was resistant to this isolate, we set out to isolate the resistance genes in WRC17 rice against the 2012-1 pathogen. The 58 RILs derived from a cross between Hitomebore and WRC17 segregated into 52 resistant and 6 susceptible lines (Fig. 1*A*), indicating that WRC17 likely contains more than one locus conferring resistance against 2012-1.

To identify the resistance genes, we performed whole-genome sequencing and RNA sequencing (RNA-seq) of WRC17 and conducted an association study using a bioinformatics pipeline we named "RaIDeN" (https://github.com/YuSugihara/RaIDeN) using the RILs segregating for these phenotypes (Fig. 1 and *SI Appendix*, Fig. S1). We sequenced the genomes WRC17, Hitomebore, and six RILs showing susceptibility to the isolate 2012-1 on an Illumina DNA sequencer (*SI Appendix*, Table S1) and subjected the short reads of WRC17 to de novo assembly with *DISCOVAR* (https://www.broadinstitute.org/software/discovar/blog/), resulting in the WRC17 reference genome sequence (*SI Appendix*, Table S2). We also performed RNA-seq of WRC17 leaves that had been inoculated with *M. oryzae* (2012-1). The RNA-seq reads were mapped to the WRC17 reference genome, revealing 22,561 genes expressed from the WRC17 genome. The short reads obtained from Hitomebore and six susceptible (S-) RILs were aligned to the genome sequences of the 22,561 expressed genes. We reasoned that Hitomebore and the six S-RILs share the same DNA sequences in the candidate genes responsible for their resistance that are different from the sequences in resistant WRC17 (*SI Appendix*, Fig. S1). Two types of DNA polymorphisms were considered: 1) presence/absence of the genes and 2) single-nucleotide polymorphisms (SNPs) in the genes. We identified 14 genes that were present in WRC17 but absent from Hitomebore and the six S-RILs, in addition to 839 genes with shared SNPs among Hitomebore and the S-RILs that were different from the sequences of WRC17.

From this group of 853 genes (Dataset S1), we selected resistance gene analogs (RGAs) using "RGAugury" (44), which predicts genes encoding putative NLRs, receptor-like kinases (RLKs), and receptor-like proteins (RLPs). This analysis identified 38 RGAs as the candidate genes (*SI Appendix*, Table S3). Since most rice resistance genes against *M. oryzae* reported to date are *NLR*s, we focused on 18 *NLR* (11 *CNL* and 7 *NL*)

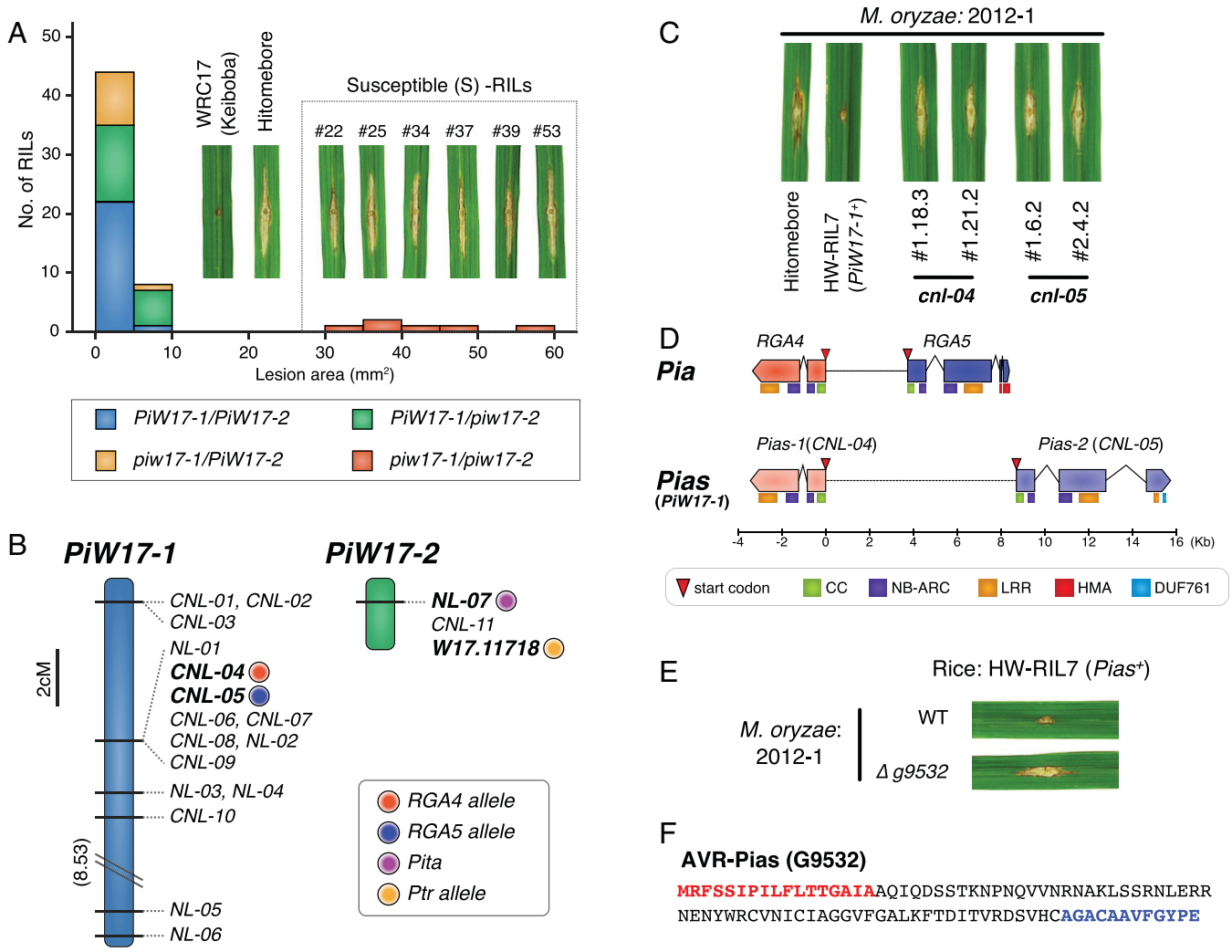

Fig. 1. *Pias* gene of rice line WRC17 (cultivar Keiboba) encodes a CC-NLR protein and is allelic to *Pia*. (*A*) Segregation of the resistance and susceptibility traits among the 58 RILs derived from a cross between WRC17 (cultivar Keiboba) and Hitomebore. Disease symptoms of WRC17, Hitomebore, and six RILs showing a susceptible phenotype after punch inoculation of *M. oryzae* isolate 2012-1 (leaf photographs) and the frequency distribution of disease lesion areas of the 58 RILs (bar graphs). (*B*) Linkage maps of candidate NLR genes at the *Pi-W17-1* and *Pi-W17-2* loci. (*C*) Both *CNL-04* and *CNL-05* are required for *Pi-W17-1*–mediated resistance against *M. oryzae* 2012-1. HW-RIL7 contains only *Pi-W17-1* and is resistant to *M. oryzae* 2012-1. Knockout of *CNL-04* (*cnl-04*) and *CNL-05* (*cnl-05*) in HW-RIL7 rendered plants susceptible to 2012-1. (*D*) Gene structures of *Pia* consisting of *RGA4* and *RGA5* and *Pias* consisting of *Pias-1* and *Pias-2*. The positions of protein domains (CC, NB-APAF-1, R-proteins and CED-4 (NB-ARC), LRR, HMA, and DUF761) encoded by the NLRs are indicated. (*E*) The *M. oryzae* 2012-1 *AVR-Pias* knockout mutant became virulent to HW-RIL7. (*F*) Amino acid sequence of G9532 protein (AVR-Pias). The secretion signal is indicated by red letters and the Toxin18-like motif is indicated by blue letters. The Toxin18-like motif was annotated by Pfam (https://pfam.xfam.org/).

genes as the candidate resistance genes of WRC17 against *M. oryzae* isolate 2012-1. Among the 18 NLR genes, only one (*NL-04*) showed presence/absence polymorphisms, and the rest contained SNPs associated with the phenotypes. We developed DNA markers in the candidate NLR genes and studied their association with phenotypes using 58 RILs segregating for resistance and susceptibility to the isolate 2012-1 (*SI Appendix*, Fig. S2*A*). This analysis showed that 16 NLRs were tightly linked to each other and that the two other *NLR*s were linked to each other, suggesting that the two loci (designated *Pi-W17-1* and *Pi-W17-2*) are involved in the resistance of WRC17 against 2012-1 (Fig. 1*B*). Genotyping of the 52 RILs using the markers located in the two loci, *Pi-W17-1* (*CNL-04*) and *Pi-W17-2* (*NL-07* and *W17.11718*), suggested that the lines became resistant when either of the two loci contained the WRC17-type allele (Fig. 1*A* and *SI Appendix*, Fig. S2*A*).

The genomic position of *Pi-W17-1* corresponds to that of the previously reported *Pia* locus (25), and the position of *Pi-W17-2* corresponds to that of the *Pita* (=*NL-07*) and *Ptr* (=*W17.11718*) loci (36, 45, 46). Among the progeny showing resistance against 2012-1, we selected 19 RILs containing *Pi-W17-1* but not *Pi-W17-2*. These lines shared 10 candidate NLR genes within the *Pi-W17-1* region (Fig. 1*B* and *SI Appendix*, Fig. S2*B*). We performed RNA interference (RNAi)–mediated gene silencing of eight of these genes (encoding proteins over 900 amino acids long) (*SI Appendix*, Fig. S2*C*) using the RIL HW-RIL7, which contains *Pi-W17-1* but lacks *Pi-W17-2*. When *CNL-04* or *CNL-05* was silenced, its resistance against 2012-1 became compromised (*SI Appendix*, Fig. S2*C* and *D*). We confirmed this result by generating *CNL-04* and *CNL-05* knockout mutant lines by CRISPR-Cas9–mediated genome editing (Fig. 1*C* and *SI Appendix*, Fig. S3). These data suggest that *Pi-W17-1*–mediated resistance requires both the neighboring NLRs *CNL-04* and *CNL-05*. Indeed, the position of *CNL-04* corresponds to that of *RGA4*, whereas the position of *CNL-05* corresponds to that of *RGA5* of *Pia* (Fig. 1*D*) (25). Interestingly, *CNL-04* is similar to *RGA4* in terms of both structure and DNA sequence (96.6%

DNA sequence identity), whereas *CNL-05* has a distinct structure and a DNA sequence that diverged from *RGA5* (59.8% DNA sequence identity) (*SI Appendix*, Fig. S4). *Pia RGA5* encodes a protein with an HMA domain in its C terminus (25), whereas *CNL-05* encodes a protein with a 19–amino acid motif corresponding to domain of unknown function 761 (DUF761) near its C terminus. The physical distance between *CNL-04* and *CNL-05* is 8.7 kb, which is longer than that between *RGA4* and *RGA5* (3.7 kb) (Fig. 1*D*). In view of the substantial differences between *CNL-05* and *RGA5*, we decided to name this WRC17 allele *Pias*, *CNL-04* as *Pias-1*, and *CNL-05* as *Pias-2* (*SI Appendix*, Fig. S5).

To isolate the *AVR-Pias* avirulence gene cognate of rice NLR *Pias*, we performed an association study of expressed genes encoding candidate effector proteins (see *SI Appendix*, Fig. S6 and Tables S4 and S5 for details). This analysis identified three genes (*G9141*, *G9435*, and *G9532*) as candidates of *AVR-Pias*. We selected *M. oryzae* isolate Ao92-06-2, which is compatible with HW-RIL7, transformed it with each of the candidate genes, and tested their interactions with HW-RIL7 (*SI Appendix*, Fig. S7). Transformation with one of the candidate genes, *G9532*, rendered Ao92-06-2 incompatible with HW-RIL7 (*SI Appendix*, Fig. S7*A*), suggesting that *G9532* is *AVR-Pias*. To validate this result, we generated a knockout mutant of *G9532* in the 2012-1 background, which became compatible with HW-RIL7 (Fig. 1*E* and *SI Appendix*, Fig. S8). These results indicate that *G9532* is *AVR-Pias*, which is recognized by *Pias*. Both *Pias-1* and *Pias-2* are required for the recognition of *AVR-Pias*, as knockout of either NLR gene abrogated resistance (*SI Appendix*, Fig. S7*B*). AVR-Pias is a 91–amino acid protein with a secretion signal peptide (Fig. 1*F*). This protein contains a 12–amino acid Toxin18-like motif (a feature of proteins belonging to the conotoxin O superfamily) in its C terminus.

Various Host Domains Are Integrated into Pias/Pia Sensor NLRs. *Pias* and *Pia* are allelic to each other, and both are composed of a pair of NLRs. The helper NLRs (*Pias-1* and *RGA4*) are conserved, whereas the sensor NLRs (*Pias-2* and *RGA5*) are divergent, with different integrated domains. To explore the diversity and evolution of *Pias/Pia* NLRs in the entire *Oryza* genus, we obtained the genomic DNA sequences of the *Pias/Pia* locus from 171 accessions representing 11 *Oryza* species as well as 4 non-*Oryza* species of Poaceae, including *Setaria italica* (foxtail millet), *Panicum hallii* (Hall's panicgrass), *Hordeum vulgare* (barley), and *Aegilops tauschii* (Tausch's goatgrass) (Dataset S2). To validate the gene structures, we used *RGA4/RGA5* and *Pias-1/Pias-2* genes as well as gene models supported by RNA-seq for 10 *Oryza* accessions as queries to infer the gene models of 167 *Oryza* accessions and 4 non-*Oryza* species using Exonerate software (www.ebi.ac.uk/~guy/exonerate) (Datasets S3 and S4). The details of the gene model prediction pipeline and the results of RNA-seq alignment to the *Pias-2/RGA5* genes are given in *SI Appendix*, Fig. S9. Remarkably, Pias-2/RGA5 sensor proteins contain a wide variety of IDs, with up to nine different domains, including HMA, DUF761, DUF677, Zinc_ribbon_12, PKc_MAPKK (PKc_M), PKc_like, and WRKY, inserted into a similar position after the LRR domain (Fig. 2*A*). Around the junction of the ID-containing fragment and the LRR domain, we identified a conserved 145– to 146–amino acid motif (Fig. 2*B*), which spans the four LRRs (LRR-9 to LRR-12). This junction region partially overlaps but is different from the previously reported CID motif (*SI Appendix*, Fig. S10) (32). Pias-2 contained a 441–amino acid fragment with six LRRs and the DUF761 ID downstream of this junction sequence (*SI Appendix*, Fig. S5).

We studied the frequency of different IDs in the 11 *Oryza* species used to reconstruct a phylogenetic tree based on whole-genome sequences (Fig. 2*C* and Datasets S2 and S4). The IDs of the cultivated rice *O. sativa* (44 samples) are shared by the HMA and DUF761 domains with similar frequencies. *O. rufipogon* (13 samples), the wild progenitor of *O. sativa*, contains DUF677 and PKc_M in addition to HMA and DUF761. *Oryza* species belonging to the A-genome group (*O. sativa*, *O. rufipogon*, *O. barthii*, *O. glumaepatula*, and *O. meridionalis*) contain a higher proportion of the DUF761 ID, suggesting its importance in their defense. However, outside the A-genome species, the DUF761 ID is absent. Instead, PKc_M (*O. brachyantha* and *O. punctata*), DUF677 (*O. officinalis*), and HMA (*O. australiensis*) are dominant, indicating that the integration of the DUF761 domain–containing fragment into Pias-2/RGA5 likely occurred in the immediate ancestor of the A-genome species that diverged from other *Oryza* lineages over 2.3 million y ago (TimeTree; www.timetree.org/).

A comparison of the genome sequences around *Pias/Pia* sensor-NLR genes between *O. punctata* and *O. sativa* cultivar Nipponbare revealed an interesting conserved region (Fig. 2*D* and *E*). Both of their coding regions contain the conserved junction sequences, whereas the IDs downstream of this sequence are different: PKc_M for *O. punctata* W1582 and DUF761 for *O. sativa* Nipponbare. However, in the 30.8-kb region downstream of the *O. sativa* Nipponbare *Pias-2* gene, two regions (blocks a and b) share high DNA sequence similarity with the junction and ID regions of the *O. punctata* W1582 *Pias-2* homolog (Fig. 2*D* and *E* and *SI Appendix*, Fig. S11): Block a corresponds to the junction region to exon-6, and block b corresponds to exon-7 to -10 of the *O. punctata* W1582 *Pias-2* homolog. Perhaps this conserved sequence downstream of the *O. sativa* Nipponbare *Pias* sensor is a footprint of the replacement of the ID from PKc_M to the DUF761-containing fragment via homologous recombination at the junction region (Fig. 2*F*). A survey of 51 A-genome *Oryza* accessions with the DUF761 ID revealed that the *O. punctata* W1582 junction–ID–like sequence is widely conserved in *O. sativa*, *O. rufipogon*, *O. meridionalis*, and an accession of *O. barthii* (accession W1702) but not in the majority of *O. barthii* and *O. glumaepatula* accessions (*SI Appendix*, Fig. S12 and Table S6). These results indicate that this possible recombination occurred only once and that the footprint was probably lost in the latter two species. We did not detect similar footprints in other sensor *Pias/Pia* NLRs with non-DUF761 IDs.

Contrasting Patterns of Evolution of *Pias/Pia* Sensors and Helpers. To explore the evolutionary patterns of the *Pias/Pia* NLR locus, we reconstructed phylogenetic trees of *Pias/Pia* NLR pairs separately for the helper NLR (Pias-1 and RGA4) and the sensor NLR (Pias-2 and RGA5) using the amino acid sequences of the helper NLRs (full-length protein) and sensor NLRs (full-length protein except the ID domain) of 22 *Oryza* accessions and 4 accessions from other Poaceae genera. Note that Pias/Pia helper and sensor NLRs belong to distantly related NLR clades (32). Overall, the helper-NLR tree (Fig. 3*A*) is consistent with the species tree (Fig. 2*C*) with a few exceptions. Species in the AA-genome group (*O. sativa* subsp. *japonica*, *O. sativa* subsp. *indica*, *O. rufipogon*, *O. barthii*, *O. glumaepatula*, and *O. meridionalis*) clustered together. Only the placement of *O. australiensis* (accession W0008) is not congruent between the Pias-1/RGA4 helper-NLR tree and the species tree. On the other

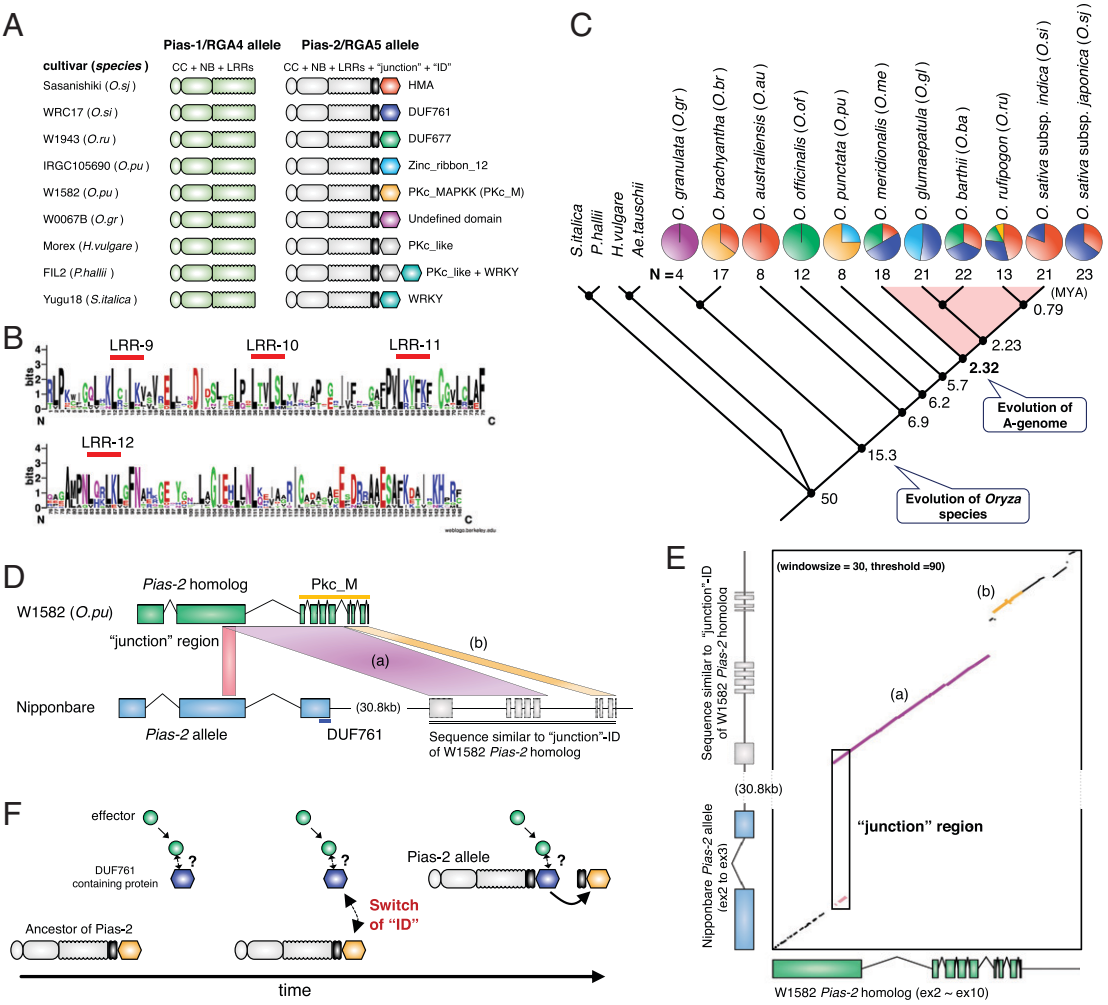

Fig. 2. Recurrent integration of extraneous domains in Pias/Pia sensor NLRs. (*A*) A simplified scheme of the structures of the Pias/Pia NLR pairs. Pias-1/RGA4 helper NLRs are shown in green, and Pias-2/RGA5 sensor NLRs are shown in white. The conserved junction sequences are indicated by gray shading. Fragments containing the IDs are shown by different-colored hexagons. (*B*) A sequence logo showing conserved amino acids of the junction motif. The red lines indicate LRRs. (*C*) Distribution of ID motifs among *Oryza* species. The pie charts show the frequencies of different ID motifs in a given species. The colors correspond to the ID colors in *A*. The numbers below the pie charts indicate the sample numbers. A cladogram showing the phylogenetic relationships of 11 *Oryza* species and 4 other Poaceae species (*S. italica*, *P. hallii*, *H. vulgare*, and *A. tauschii*) based on TimeTree, the Timescale of Life web database (www.timetree.org/). The numbers on the branches indicate the estimated time of the splitting of lineages (MYA, million y ago). (*D*) DNA sequence similarity between the *O. punctata Pias-2/RGA5* sensor NLR and the downstream sequence of the *O. sativa* (Nipponbare) *Pias-2/RGA5*. (*E*) Dot-plot analysis of the *O. punctata* (W1582) *Pias-2/RGA5* sensor NLR and *O. sativa* (Nipponbare) *Pias-2/RGA5* NLR downstream sequences using the Dotmatcher tool (emboss.bioinformatics.nl/cgi-bin/emboss/dotmatcher/). (*F*) Possible evolutionary process of ID replacement that might have occurred between the *O. punctata* and the *O. sativa Pias-2/RGA5* lineages. We still do not know the mode of interaction between the AVR-Pias effector and DUF761-containing protein, so it is indicated by "?.".

hand, the sensor-NLR tree is quite distinct from the helper-NLR tree and is not congruent to the species tree. Remarkably, the sensor NLRs show a higher level of divergence than the helper NLRs (Fig. 3*A*). The sensor phylogeny includes two major clades (C1 and C2) separated by deep branches. RGA5 of *O. sativa* cv. Sasanishiki (25) belongs to the C1 clade, whereas Pias-2 of *O. sativa* WRC17 belongs to the C2 clade. Four species of the AA-genome group (*O. sativa* subsp. *japonica*, *O. sativa* subsp. *indica*, *O. rufipogon*, *O. barthii*, and *O. meridionalis*) and *O. punctata* (BB genome) have sensor-NLR alleles from both the C1 and C2 clades, whereas *O. australiensis* (EE genome), *O. granulata* (GG genome), and *O. brachyantha* (FF genome) have C1 alleles, and *O. glumaepatula* (AA genome) and *O. officinalis* (CC genome) have C2 alleles. Therefore, phylogenetic analysis of the sensor NLR of the *Pias/Pia* locus pointed to a transspecies polymorphism, which is reminiscent of the major histocompatibility (MHC) gene polymorphism in vertebrates (47).

To determine whether the paired NLRs have accumulated mutations at different rates, we calculated the nucleotide diversity and Tajima's *D* (48). The nucleotide diversities of the *Pias-2/RGA5* sensor were markedly higher than those of the *Pias-1/RGA4* helper for each of the CC, nucleotide binding site (NBS), and LRR(-LII) domains (Fig. 3*B*). Also, the three domains of the *Pias-1/RGA4* helper and *Pias-2/RGA5* sensor had contrasting negative and positive Tajima's *D*, respectively (Fig. 3*C*), indicating purifying selection in *Pias-1/RGA4* and balancing selection in *Pias-2/RGA5*, especially in the LRR domain. These results suggest that the genetically linked helper and sensor NLRs of the *Pias/Pia* locus in the genus *Oryza* have undergone contrasting modes of evolution.

To determine the types of nucleotide substitutions in the *Pias-1/RGA4* helper and *Pias-2/RGA5* sensor, we calculated d_N (nonsynonymous mutations) and d_S (synonymous mutations) (Fig. 3*D*). Consistent with higher nucleotide diversity and Tajima's *D*, we noted overall higher d_N and d_S in *Pias-2/RGA5*, notably in the NBS and LRR domains (Fig. 3*D*). We also observed that the pairwise d_N and d_S of *Pias-1/RGA4* were constrained by the low genetic divergence in many of the examined pairs. Nonetheless, d_S was higher in *Pias-1/RGA4* for the CC

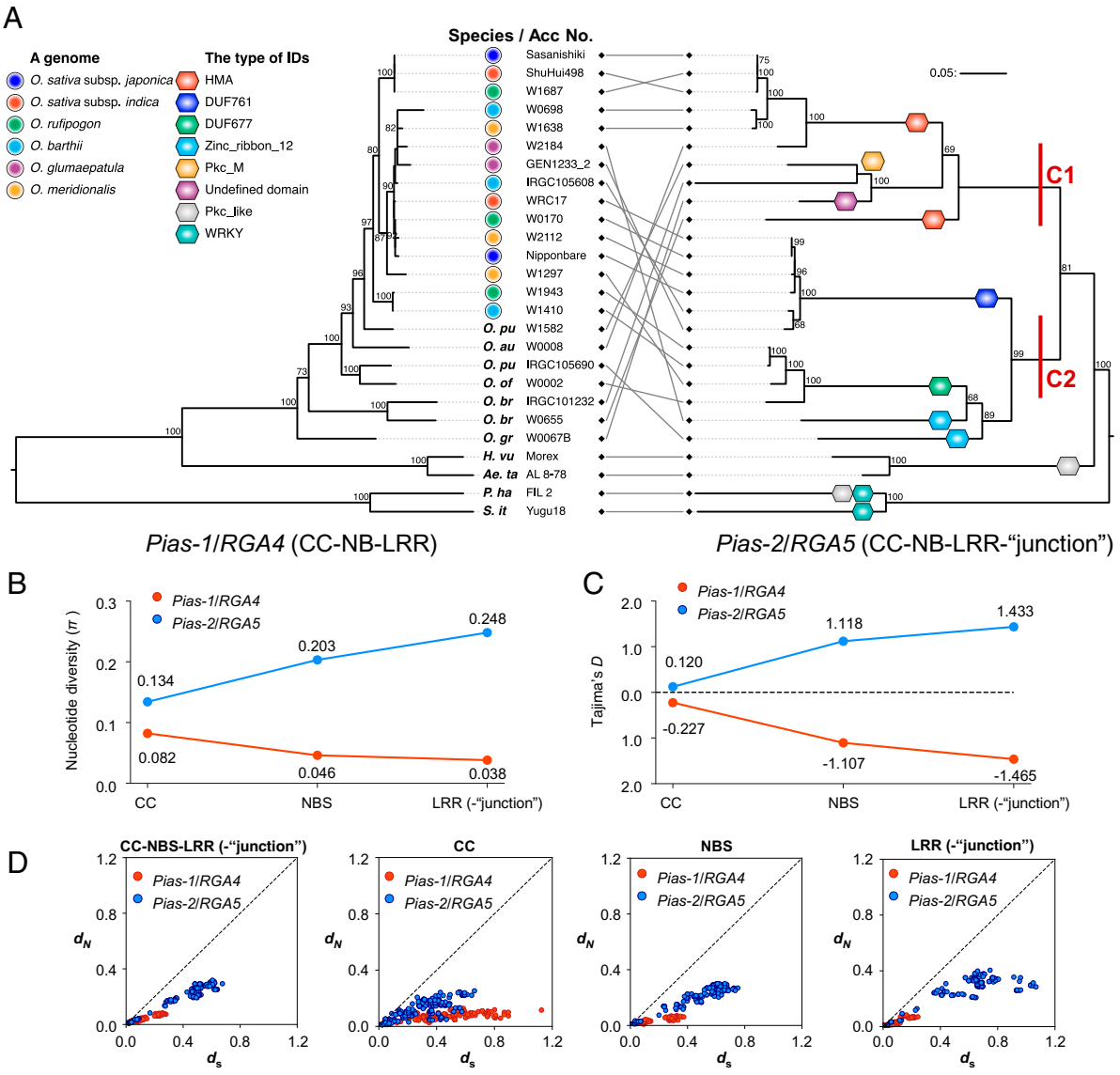

Fig. 3. Contrasting evolutionary patterns of the helper and sensor NLRs of the *Pias/Pia* locus. (*A*) Phylogenetic tree of the *Pias-1/RGA4* helper-NLR gene (*Left*) and *Pias-2/RGA5* sensor-NLR (*Right*) gene based on the full-length amino acid sequence of Pias-1/RGA4 and the sequence in the region CC to the junction region for Pias-2/RGA5. *Pias-2/RGA5* sensor NLRs form two major clades (C1 and C2). The numbers indicate bootstrap values. (*B*) Nucleotide diversity (π) of the CC, NBS, and LRR(-junction region) domains of the *Pias-1/RGA4* helper-NLR gene and *Pias-2/RGA5* sensor-NLR gene in 22 *Oryza* samples. (*C*) Tajima's *D* of the CC, NBS, and LRR(-junction region) domains of the *Pias-1/RGA4* helper-NLR gene and *Pias-2/RGA5* sensor-NLR gene in 22 *Oryza* samples. (*D*) Pairwise d_N and d_S values of the CC-NBS-LRR(-junction region), CC, NBS, and LRR domains of the *Pias-1/RGA4* helper-NLR gene and *Pias-2/RGA5* sensor-NLR gene in 22 *Oryza* samples.

domain than in *Pias-2/RGA5* (Fig. 3*D* and *SI Appendix*, Fig. S13). These results suggest that different evolutionary patterns affect the different domains of *Pias-1/RGA4* and *Pias-2/RGA5*.

The Pias-1 Helper Functions with the RGA5 Sensor to Recognize AVR-Pia. Pia comprises the helper-NLR RGA4 and the sensor-NLR RGA5. The expression of RGA4 triggers HR cell death in rice as well as *N. benthamiana*, and RGA5 suppresses RGA4-mediated cell death (49). Upon the binding of AVR-Pia to the HMA ID of RGA5, this suppression is released, and HR-like cell death is triggered (49). To address the functional conservation of helper/sensor NLRs of the *Pias/Pia* locus, we examined the functions of helper NLRs by transiently overexpressing five Pias/Pia helper NLRs in *N. benthamiana* using agroinfiltration (*SI Appendix*, Fig. S14). Only RGA4 supported strong cell death, and other alleles including Pias-1 caused weaker cell death, indicating that the role of RGA4 as a strong HR inducer is not typical among the tested helper NLRs (*SI Appendix*, Fig. S14). Next, we tested the effects of coexpressing Pias-1 and Pias-2, which surprisingly resulted in stronger cell death than that caused by Pias-1 expression alone (*SI Appendix*, Fig. S15). Coexpression of AVR-Pias with Pias-1 and Pias-2 did not alter the level of cell death (*SI Appendix*, Fig. S15). A coimmunoprecipitation analysis showed that Pias-1 and Pias-2 interact (*SI Appendix*, Fig. S16), and a yeast two-hybrid assay showed that the CC domains of Pias-1 and Pias-2 form homo- and heterodimers (*SI Appendix*, Fig. S16). These results suggest that Pias-1 and Pias-2 physically interact like RGA4/RGA5, but their mode of action is different from that of the RGA4/RGA5 pair.

We next examined the effects of exchanging various helper and sensor Pias/Pia NLRs by performing a transient expression assay in *N. benthamiana* leaves (Fig. 4*A* and *SI Appendix*, Fig. S17). Coexpression of the sensor RGA5 with the two heterologous helpers (Pias-1 and RGA4-Ogr from *O. granulata*) suppressed HR-like cell death, indicating that RGA5 can suppress the cell death induced by helper NLRs other than RGA4 (Fig. 4*A* and *SI Appendix*, Fig. S17). Furthermore, this RGA5-mediated suppression of the Pias-1–triggered HR was released via coexpression of

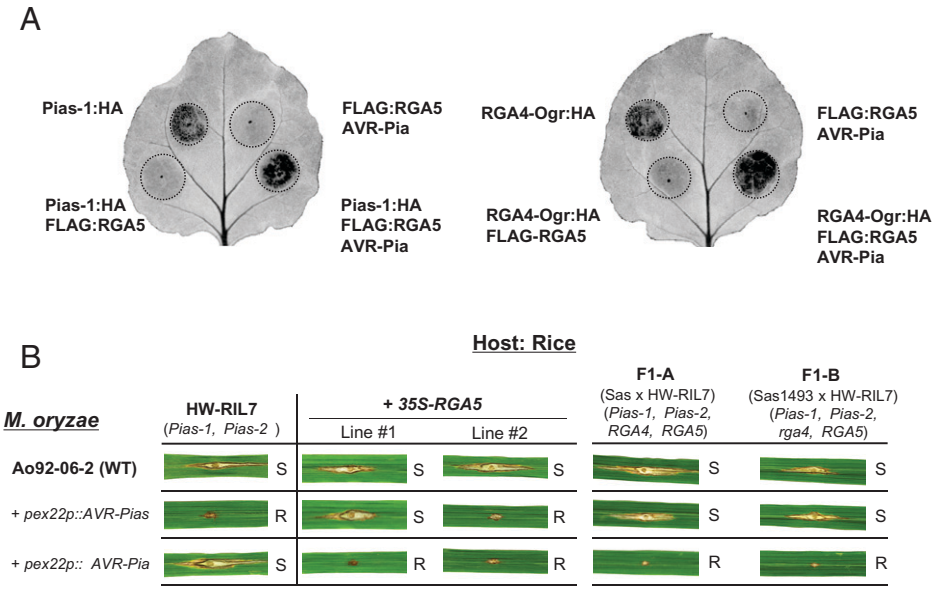

Fig. 4. NLR-helper Pias-1 is functionally conserved. (*A*) Representative images of *N. benthamiana* leaves after agroinfiltration with Pias-1:HA, Pias-1:HA/FLAG:RGA5, FLAG:RGA5/AVR-Pia, and Pias-1:HA/FLAG:RGA5/AVR-Pia (*Left*) and RGA4-Ogr:HA derived from *O. granulata*, RGA4-Ogr:HA/FLAG:RGA5, FLAG:RGA5/AVR-Pia, and RGA4-Ogr:HA/FLAG:RGA5/AVR-Pia (*Right*). Autofluorescence under UV light is shown. (*B*) Pias-1 cooperates with RGA5 to recognize AVR-Pia and induces resistance in rice. The rice line HW-RIL7 with *Pias* (*Pias-1* and *Pias-2*) recognizes the Ao-92-06-2 strain with *AVR-Pias* (Ao92-06-2+*pex22p:AVR-Pias*) and induces resistance. However, HW-RIL7 cannot recognize the Ao02-06-2 strain with *AVR-Pia* (Ao92-06-2+*pex22p:AVR-Pia*). Two lines (lines 1 and 2) contain the *35S-RGA5* transgene in the HW-RIL7 background. F1-A is a progeny derived from a cross between Sasanishiki with *Pia* (*RGA4* and *RGA5*) and HW-RIL7. F1-B is a progeny derived from a cross between a Sasanishiki mutant (Sas1493) with *pia* (*rga4* and *RGA5*) and HW-RIL7. "R" and "S" indicate resistance and susceptibility, respectively.

AVR-Pia, which resulted in cell death (Fig. 4*A* and *SI Appendix*, Fig. S17). A similar result was obtained using the RGA4-Ogr helper (Fig. 4*A* and *SI Appendix*, Fig. S17). These results indicate that the sensor RGA5 properly functions with helpers other than RGA4 to recognize AVR-Pia and mount the HR in *N. benthamiana*.

Finally, we generated transgenic rice plants (HW-RIL7:35S-RGA5) expressing the *RGA5* transgene driven by the 35S cauliflower mosaic virus (CaMV35S) promoter in the *Pias* (*Pias-1* and *Pias-2*) background. We challenged these lines with two *M. oryzae* isolates: Ao92-62-2 harboring the *AVR-Pia* transgene and Ao92-62-2 harboring the *AVR-Pias* transgene (Fig. 4*B* and *SI Appendix*, Fig. S18). Remarkably, HW-RIL7:35S-RGA5 exhibited resistance against *M. oryzae* containing *AVR-Pia* (Fig. 4*B*). Although the HW-RIL7:35S-RGA5 lines consistently showed resistance against *M. oryzae* containing *AVR-Pia*, their resistance against *M. oryzae* containing *AVR-Pias* varied. We crossed an *rga4* mutant in the Sasanishiki background [Sas1493 (25)] with HW-RIL7 and obtained F1-B plants. These plants, harboring intact *RGA5* as well as *Pias-1* and *Pias-2*, now recognized and triggered resistance against *M. oryzae* containing *AVR-Pia* but not *AVR-Pias* (Fig. 4*B*). Similar results were obtained for F1-A plants generated by crossing Sasanishiki (wild type; WT) with HW-RIL7 (Fig. 4*B*). These results suggest that *Pia* function is dominant over *Pias* function in terms of the recognition of *AVR-Pia* and *AVR-Pias*.

These results suggest that the Pias-1 helper functions together with RGA5 in rice to recognize and mount resistance against *M. oryzae* containing *AVR-Pia*, suggesting that the helper function has been conserved over the long history of Pias/Pia evolution.

Discussion

Our study investigated the evolution of a pair of genetically linked NLRs in the genus *Oryza* and provided experimental evidence that the two paired NLRs have evolved in dramatically contrasting fashions. This study points to the evolution of a modular architecture of paired NLRs. Division of roles between a conserved helper NLR for signaling and a divergent sensor NLR with a cassette-like receptor domain for pathogen sensing may have given plants the ability to efficiently fend off rapidly evolving microbe pathogens.

We identified and functionally characterized the rice *R* gene *Pias*. This gene encodes the paired NLRs Pias-1 helper and Pias-2 sensor, which recognize the *M. oryzae* effector AVR-Pias. *Pias* is allelic to the well-studied *R* gene *Pia*, encoding the NLRs RGA4 helper and RGA5 sensor (25), which recognizes the effectors AVR-Pia (50) and AVR1-CO39 (26). The allelic sensor-NLRs Pias-2 and RGA5 carry different domains at their C termini. In RGA5, the integrated domain HMA directly binds to and recognizes two *M. oryzae* effectors, AVR-Pia and AVR1-CO39 (26). We have not yet detected direct binding between the DUF761 ID of Pias-2 and AVR-Pias despite several attempts. Perhaps the recognition of AVR-Pias by Pias-2 requires other host components; indeed, the recognition of AVR-Pii by Pii-2 requires the rice protein OsExo70-F3, which binds to both AVR-Pii and Pii-2 (30, 39).

What is the origin of the integrated DUF761 domain of Pias-2? The rice sensor-NLRs RGA5 and Pik-1 contain HMA domains as IDs. The ID HMA shares high amino acid sequence similarity with rice small heavy metal–associated domain proteins [sHMAs (51, 52)]. We revealed that the *M. oryzae* effector AVR-Pik binds to and stabilizes sHMA proteins, likely to promote pathogen infection (51, 53). To identify the proteins that provide the DUF761 domain to the Pias-2 ID, we performed BLAST searches against the rice protein database using the short Pias-2 DUF761 sequence (19 amino acids) as a query (*SI Appendix*, Fig. S19). This identified 15 proteins with a similarity threshold of E <10. Most of the 15 proteins contained DUF761 at their C termini. Only a few functional studies of DUF761-containing proteins have been performed. A study in cotton (*Gossypium hirsuta*) showed that GhCFE1A, containing DUF761 and DUF4408 domains, binds to actin proteins and localizes to the endoplasmic

reticulum (ER) upon overexpression in *N. benthamiana* (54). Knockdown of *GhCFE1A* did not cause any phenotypic changes, while its overexpression led to delayed cotton fiber cell elongation. These results suggest that GhCFE1A is a linker protein that mediates the formation of the ER network and actin cytoskeleton. *Arabidopsis A70*, encoding a DUF761-containing protein, is specifically induced in the incompatible interaction with *Pseudomonas syringae*, but not in the compatible interaction (55). Knockout of the *Arabidopsis* DUF761-containing protein gene *DUF761-1* did not have any phenotypic effects, whereas overexpressing *DUF761-1* altered plant morphology and resulted in a constitutive defense response, leading to enhanced resistance against *P. syringae* (56). These findings suggest that DUF761-containing proteins function in defense, presumably mediated by the actin–ER network. Previous studies of the NLRome of *Arabidopsis* (6) and NLR-ID of various members of the plant kingdom (8) showed that DUF761 is one of the most common domains integrated into NLRs as the ID. In *Arabidopsis*, DUF761 was integrated into TIR-NLR, and the NLRs with DUF761-ID are in almost all cases paired with helper NLRs (6). These findings suggest that the DUF761 domain is a major target of pathogen effectors and has been frequently integrated into NLRs. Future studies should investigate how AVR-Pias is recognized by Pias and how AVR-Pias interferes with host cellular processes by its possible interaction with DUF761-containing proteins.

Divergent Sensor NLRs in the Pias/Pia Lineage. The Pias-2/RGA5 sensor-NLR lineage is extremely divergent among *Oryza* species, with up to six different ID motifs integrated at their C termini (Fig. 2). These hugely divergent IDs may mediate the detection of a diversity of effectors from the blast fungus and possibly other pathogens. We hypothesize that the diversity of the Pias-2/RGA5 lineage has been maintained by natural selection to maintain various IDs that recognize the invasion of pathogens by directly binding to effectors or guarding host factors that are modified by effectors.

Within *Oryza* species, there are two major clades, C1 and C2. Notably, alleles from both clades are maintained within the species *O. sativa*, *O. rufipogon*, *O. barthii*, *O. meridionalis*, and *O. punctata*. The observed transspecies allelic divergence and their roles in detecting pathogen molecules are similar to those of the MHC locus of vertebrates (47). Individuals with higher heterozygosity at the MHC locus might have higher fitness (overdominance) due to their ability to bind to a larger number of pathogen peptides (57, 58). Perhaps in the ancestral outcrossing *Oryza* species, heterozygous plants with a larger repertoire of NLRs with different IDs had a selective advantage against a multitude of pathogens. It is also possible that frequency-dependent selection helped maintain this polymorphism. When the frequency of a pathogen effector in a population increases, the frequency of an allele for a cognate sensor NLR will increase, resulting in a reduction in the frequency of pathogen alleles in the population. In turn, the frequency of another effector gene will increase in the pathogen, and the frequency of the cognate sensor NLR will increase. According to this Red Queen model, the allele frequencies of both effector and sensor NLRs oscillate and may be maintained for a long time by balancing selection (57, 59, 60). In summary, the highly divergent evolution of Pias/Pia sensor NLRs with variable IDs seems driven by the fitness gain obtained by an enhanced recognition capability of pathogen effectors.

Genetic Mechanism of ID Switching in Pias/Pia NLRs. The Pias/Pia sensor NLRs contain various ID sequences at the similar position downstream of the LRR domain. This suggests the presence of a mechanism for "cassette"-like exchange of IDs between sensor NLRs. In the upstream region of the ID, we identified a highly conserved stretch of 145–amino acid sequences. A recent study reported a 43–amino acid CID motif conserved in the region between the LRR and ID of the MIC1 NLR clade by studying the NLRs of seven Poaceae species (32). The conserved region identified here encompasses the CID motif (*SI Appendix*, Fig. S10) but extends in the N-terminal direction by ∼100 amino acids including four LRRs. The authors hypothesized that the CID could serve as a recombination point of integration of genomic sequences. Despite the difference in the conserved motif, our data basically support the hypothesis that this region serves as the recombination point for the integration of endogenous sequences matching various protein domains. In support of this idea, the downstream sequence of a Pias sensor NLR with DUF761 contains a DNA sequence similar to the junction and ID regions of the *O. punctata* Pias sensor homolog. Perhaps the PKc_M ID of the original *O. punctata* Pias was replaced by the DUF761 ID–containing fragment, and this switch caused the translocation of PKc_M to the region downstream of the sensor-NLR gene (Fig. 2*F*). In view of the high sequence conservation between the *O. punctata* PKc_M ID and the downstream sequence, it is also possible that the downstream sequence was functional until the recent past, the Pias sensor contained the dual IDs DUF761 and PKc_M in the same molecule, or Pias switched between these two IDs, possibly via alternative splicing. Future studies should address the mechanism of the junction sequence-mediated recombination.

Function of *Pias/Pia* Paired NLRs. Pia has been extensively studied (49) and serves as a paradigm for paired NLRs together with the paired NLRs RPS4/RRS1 (23). In these two cases, the helper NLR is regarded as a cell-death inducer and the sensor NLR as a suppressor that maintains the complex in an inactive state when the pathogen is absent. Once the sensor has been modified by direct binding (RGA5) or modification (RRS1) of the ID by pathogen effectors, the suppression of the helper is released and HR-like cell death occurs. However, Pias NLRs do not function according to this model. In the *N. benthamiana* assay, Pias-1 functioned as a weak cell-death inducer and Pias-2 did not suppress Pias-1–mediated cell death. Indeed, Pias-1 and Pias-2 together triggered stronger cell death than that caused by Pias-1 alone. A recent functional study of rice Pikp, another paired NLR, also showed that the helper NLR alone does not cause cell death in the *N. benthamiana* system and that the helper and sensor cooperate to trigger HR (42). Therefore, the hypothesized functional roles of the helper as a cell-death inducer and the sensor as a cell-death suppressor as well as a detector of effector molecules may not be as prevalent as assumed. The system of negative regulation of a cell-death inducer by a suppressor encoded by genetically separate factors carries tremendous risks given that a loss-of-function mutation in the suppressor gene kills the carrier cells and incurs a genetic load. Therefore, such an extreme negative regulation system is unlikely to be maintained over a long period of evolution. We predict that cooperative NLRs in pairs or networks are more prevalent (31). It is also possible that the Pias/Pia-paired NLR system is regulated by additional components in rice cells that are absent from *N. benthamiana*. It would be interesting to experimentally determine what proportions of paired NLRs function in negative regulation and in cooperation using *N. benthamiana* transient expression assays. Further studies are needed to decipher the full regulatory network of Pias/Pia-paired NLR-mediated resistance.

Helper NLRs in the Pias/Pia Lineage Are Functionally Conserved. Phylogenetic reconstruction of the Pias/Pia NLR locus revealed that the helper-NLR Pias-1/RGA4 is conserved, whereas the sensor-NLR Pias-2/RGA5 is highly divergent (Fig. 3). An *Arabidopsis* NLRome study showed that some NLR pairs coevolved, with the phylogenetic trees of helper and sensor NLRs corresponding (6). Our findings for Pias/Pia NLRs do not align with these observations. A functional study in *N. benthamiana* showed that Pias-1–mediated cell death was suppressed by RGA5 and that Pias-1 together with RGA5 functions in the recognition of AVR-Pia, leading to cell death (Fig. 4*A*). Similarly, an RGA4 homolog of *O. granulata* that is phylogenetically distant from *O. sativa* also functions with RGA5 to recognize AVR-Pia (Fig. 4*A*). Moreover, an HW-RIL7 rice line harboring *Pias* as well as an *RGA5* transgene recognized AVR-Pia (Fig. 4*B*). These results suggest that the function of the Pias-1/RGA4 helper lineage is conserved, which is in line with its conserved amino acid sequences. It is possible that the separation of the roles of NLRs between the conserved helper and divergent sensor allowed for higher flexibility of pathogen recognition compared with singleton NLRs. This flexibility would allow the plant to cope with the rapid evolution of pathogens, which exhibit larger population sizes and shorter generation times than the host plants. The functional understanding of the modular structure of paired NLRs revealed here provides a basis for engineering NLRs to detect various effectors and to confer resistance to crops against pathogens.

Materials and Methods

Rice Pathogenicity Assays. Rice leaf blade punch inoculation was performed using the *M. oryzae* isolates. A conidial suspension (3×10^5 conidia per milliliter) was punch-inoculated onto a rice leaf 1 mo after seed sowing. The inoculated plants were placed in a dew chamber at 27 °C for 24 h in the dark and transferred to a growth chamber with a 16-h light/8-h dark photoperiod. Disease lesions were scanned 10 d postinoculation, and lesion size was measured using ImageJ software (61).

RNA-Seq of Rice and Barley Leaves Infected with *M. oryzae* 2012-1 Isolate. Total RNA was extracted from rice- and barley-infected leaves using an SV Total RNA Isolation System (Promega). One microgram of total RNA was used to prepare each sequencing library with an RNA Sample Prep Kit v2 (Illumina). The two types of libraries, created from infected barley and rice leaves, were sequenced by paired-end (PE) and single-end (SE) sequencing using the NextSeq 500 platform.

DNA-Seq for the RaIDeN Pipeline. Genomic DNA was extracted from WRC17, Hitomebore, and S-RIL leaves using a NucleoSpin Plant II Kit (Macherey Nagel). Libraries for PE short reads were constructed using a TruSeq DNA LT Sample Prep Kit (Illumina). The PE library of WRC17 and other libraries were sequenced on the Illumina MiSeq and HiSeq 4000 platforms.

Generation of *Pi-W17-1* with Knocked-Down Expression of Candidate NLR Genes in Rice and qRT-PCR. The eight types of gene knockdown (RNAi) constructs (pANDA-*Pi-W17-1* candidate NLRs) were generated by PCR amplification of a specific fragment of each *Pi-W17-1* candidate NLR gene from WRC17 WT complementary DNA (cDNA). The sequences were cloned into the Gateway vector pENTR/D-TOPO (Invitrogen) and transferred into recombination sites of the pANDA vector (62) using LR Clonase (Invitrogen). The resulting vectors with eight types of pANDA-*Pi-W17-1* candidate NLR genes were introduced into *Agrobacterium tumefaciens* (strain EHA105) and used for *A. tumefaciens*–mediated transformation of HW-RIL7 following the method of Okuyama et al. (25). Total RNA was extracted from leaves using an SV Total RNA Isolation System (Promega) and used for qRT-PCR. cDNA was synthesized from 500 ng total RNA using a PrimeScript RT Reagent Kit (Takara Bio). qRT-PCR was performed using a StepOne Real-Time PCR Instrument (Applied Biosystems) with KAPA SYBR FAST PCR Master Mix (Kapa Biosystems). Melting curve analysis (from 60 to 95 °C) was included at the end of the cycles to ensure the consistency of the amplified products. The comparative Ct (ΔΔCt) method was used to calculate the expression of *CNL-04* (*CNL-05*) relative to the rice *ACTIN* gene (*LOC_Os03g50885*) as an internal control. The data presented are the average and SDs from three experimental replications. The primers used to generate the RNAi construct and for qRT-PCR are listed in Dataset S5.

Generation of Rice Mutants of *CNL-04* and *CNL-05* by CRISPR-Cas9–Mediated Genome Editing. Rice knockout mutants of *CNL-04* and *CNL-05* were generated using the CRISPR-Cas9 system developed by Mikami et al. (63). Sense and antisense target sequences were designed using the web-based service CRISPRdirect (crispr.dbcls.jp), annealed, and cloned into the pU6::ccdB::gRNA cloning vector following digestion with *Bbs*I as the target sequence. The target sequence with the *OsU6* promoter was cloned into the pZH::gYSA::MMCas9 vector following digestion with *Asc*I and *Pac*I. The resulting vectors (pZH::gYSA::MMCas9-*CNL-04* and -*CNL-05*) were introduced into *A. tumefaciens* (strain EHA105) and used for *A. tumefaciens*–mediated transformation of HW-RIL7 following the method of Okuyama et al. (25). The resulting regenerated T_0 plants were sequenced, and the mutation type was confirmed using primers listed in Dataset S5.

Genetic Complementation of the Candidate AVR-Pias. Three candidate gene constructs (pCB1531-*AVR-Pias* candidate) were generated by PCR amplification of the coding sequences of the *AVR-Pias* candidate genes from cDNA prepared from *M. oryzae* 2012-1–infected barley leaves. The sequences were digested with *Xba*I and *BamH*I and cloned into pCB1531-pex22p-EGFP following the method of Yoshida et al. (50) that had been linearized by digestion with *Xba*I and *BamH*I. The resulting vectors were used to transform Ao92-06-2 (lacking *AVR-Pias*) following the method of Sweigard et al. (64). *M. oryzae* isolate 2012-1 mutated in *G9532* was generated using the CRISPR-Cas9 system developed by Arazoe et al. (65). Sense and antisense target sequences were designed using the web-based service CRISPRdirect (crispr.dbcls.jp), annealed, and cloned into the pCRISPR-Cas-U6-1 cloning vector following the method of Arazoe et al. (65). To generate the targeting vector TV-*G9532*, the 5′ flanking region of *G9532* was amplified and cloned into pCB1636 (64) containing a hygromycin resistance gene that had been linearized by inverse PCR using primers pCB1636iv2fwd and pCB1636iv2rev as described by Shimizu et al. (66) using In-Fusion cloning (Clontech). Subsequently, the 3′ flanking region was amplified and cloned into a plasmid containing the 5′ flanking region that had been linearized by inverse PCR using primers pCB1636iv1fwd and pCB1636iv1rev as described by Shimizu et al. (66) using In-Fusion cloning (Clontech). The resulting vectors were used to transform the 2012-1 isolate (containing *AVR-Pias*) following the method of Sweigard et al. (64). The primers used for construct generation are listed in Dataset S5.

Genome Sequences Used for the Study. Genome sequences of 171 accessions of Poaceae plants were used, including 167 *Oryza* accessions as well as one accession each from *A. tauschii*, *H. vulgare*, *P. hallii*, and *S. italica*. These also included sequences of *O. sativa* WRC17 (this study) and *O. sativa* Sasanishiki (25). Genome sequences of 66 accessions were obtained from public databases: 52 accessions of *O. sativa* and *O. rufipogon* (67), *O. sativa* subsp. *indica* ShuHui498 (68), *O. sativa* subsp. *japonica* Nipponbare (69), *O. rufipogon* W1943 (National Center for Gene Research, Chinese Academy of Sciences, China), 5 accessions from *O. barthii*, *O. glumaepatula*, *O. meridionalis*, *O. punctata*, and *O. brachyantha* (The *Oryza* Map Alignment Project), *O. officinalis* W0002 (National Institute of Genetics, Japan), *O. granulata* W0067B (70), *A. tauschii* AL8/78 (71), *H. vulgare* Morex (72), *P. hallii* FIL2 (Department of Energy Joint Genome Institute), and *S. italica* Yugu18 (73) (see Dataset S2 for details). For 101 accessions of the wild *Oryza* species (*O. barthii*, *O. glumaepatula*, *O. meridionalis*, *O. punctata*, *O. officinalis, O. brachyantha*, and *O. granulata*), next-generation sequencing (NGS) reads (fastq format) of whole-genome sequences were retrieved from the NGS National Center for Biotechnology Information (NCBI) database (Dataset S2) and used for de novo assembly by MaSuRCA (74). For the two wild *Oryza* accessions, *O. glumaepatula* W2184 and *O. punctata* W1582, DNA sequencing was performed using Oxford Nanopore Technology (ONT) using genomic DNA extracted from their leaves. Sequencing was performed using the PromethION System with a FLO-PRO002 flow cell (ONT). Base calling of ONT reads was performed on FAST5 files using Guppy (ONT). Subsequently, low-quality reads were filtered out, and de novo assembly was performed using NECAT software (https://github.com/xiaochuanle/NECAT/). To further improve the accuracy of the assembly, Racon

software (https://github.com/lbcb-sci/racon) was applied twice, and Medaka (https://github.com/nanoporetech/medaka) was used to correct misassembly. One round of consensus correction was performed using BWA (75) and HyPo (https://github.com/kensung-lab/hypo) on Illumina short reads for the accessions.

Gene Annotation and Detection of Pias/Pia Orthologs. To infer the protein-coding regions of *Pias-1/RGA4* and *Pias-2/RGA5* genes, and to obtain information about their ID sequences, we used the pipeline shown in *SI Appendix*, Fig. S9. We retrieved *Pias-1/RGA4* and *Pias-2/RGA5* gene models from the genome sequences and RNA-seq data publicly available for seven *Oryza* samples (*O. barthii* IRGC105608, *O. glumaepatula* GEN1233_2, *O. meridionalis* W2112, *O. punctata* IRGC105690, *O. australiensis* W0008, *O. brachyantha* IRGC101232, and *O. granulata* W0067B). For *O. rufipogon* W1943 and *O. officinalis* W0002, genome sequences were publicly available, but we performed new RNA-seq analyses to improve gene prediction. For the sample *O. punctata* W1582, we performed genome sequencing and RNA-seq analyses. We also used the *RGA4/RGA5* gene model of *O. sativa* cv. Sasanishiki (25) and the *Pias-1/Pias-2* gene model of *O. sativa* cv. Keiboba (this study). The gene models of *Pias-1/RGA4* and *Pias-2/RGA5* of these 12 *Oryza* samples were used as queries to annotate IDs in the genome assembly of 167 *Oryza* samples using Exonerate (www.ebi.ac.uk/~guy/exonerate). However, 10 samples of *O. glumaepatula* and 6 samples of *O. brachyantha* did not match known domains. Therefore, we incorporated RNA-seq data for each sample for the two species, resulting in the annotation of the Zinc_ribbon_12 (*O. glumaepatula*) and HMA (*O. brachyantha*) IDs. In the next round, we used the gene models of 12 samples used in the first round of Exonerate as well as two new samples (*O. glumaepatula* W2184 and *O. brachyantha* W0655) as queries to infer IDs in the assembled genomes of 167 *Oryza* samples (Datasets S2, S3, and S4). This resulted in the identification of five known domains and one unknown domain in the *Oryza* ID sequences.

Amino Acid Sequences and Accession Numbers of Pias/Pia Orthologs. Amino acid sequences of Pias/Pia homologs used in this study were retrieved from the Eukaryotic Genome Annotation of the NCBI database; accession numbers for Pias-1/RGA4 homologs and Pias-2/RGA5 homologs are as follows: XP_015617251.1 and XP_015617810.1 for *O. sativa* subsp. *japonica* Nipponbare, OsR498G1119642600.01 and OsR498G1119642700.01 for *O. sativa* subsp. *indica* ShuHui498, XP_020148260.1 and XP_020148256.1 for *A. tauschii* AL8/78, HORVU.MOREX.r2.4HG0288000.1 and HORVU.MOREX.r2.4HG0288010.1 for *H. vulgare* Morex, XP_025826635.1 and XP_025827327.1 for *P. hallii* FIL2, and XP_004979045.1 and XP_004979046.2 for *S. italica* Yugu18.

Phylogenetic Analysis of Pias-1/RGA4 and Pias-2/RGA5 Orthologs. The protein sequences of the Pias-1/RGA4 and Pias-2/RGA5 orthologs were aligned using webPRANK (https://www.ebi.ac.uk/goldman-srv/webprank/) (76). We used the whole amino acid sequences of the Pias-1/RGA4 orthologs but only the partial amino acid sequences (CC-NB-LRR-junction domains) of the Pias-2/RGA5 orthologs due to the very low sequence similarity after the junction domains. A maximum-likelihood tree was constructed with IQ-TREE v2.0.3 (77) using 1,000 ultrafast bootstrap replicates (78). The models were automatically selected by ModelFinder (79) in IQ-TREE (77). ModelFinder (79) selected "JTT + G4" for Pias-1/RGA4 orthologs and "JTT + R2" for Pias-2/RGA5 orthologs. Finally, the phylogenetic trees were drawn with FigTree v1.2.3 (tree.bio.ed.ac.uk/software/figtree/).

Analysis of DNA Polymorphisms, d_N and d_S. The coding DNA sequences (CDSs) of the *Pias-1/RGA4* and *Pias-2/RGA5* orthologs were aligned using the codon-based aligner MACSE v2.05 (80). We applied MACSE v2.05 not only to the entire CDS of *Pias-1/RGA4* and CC-NBS-LRR-junction of *Pias-2/RGA5* but also to each domain (CC, NBS, and LRR[-junction sequence]) using default parameters. We evaluated DNA polymorphisms of the *Pias-1/RGA4* and *Pias-2/RGA5* orthologs, calculating the nucleotide diversity (π) and Tajima's *D* (48) using MEGA X v10.2.4 (81). Then, for each alignment, the maximum-likelihood trees were constructed using IQ-TREE v2.0.3 with 1,000 ultrafast bootstrap replicates (78) and ModelFinder (79). Based on these alignments and trees, we calculated the pairwise d_N and d_S using the YN00 program (82) in PAML v4.8 (83).

Expression Constructs Used in the Cell-Death Assay. Expression constructs for five types of helper NLRs, Pias-1 (*O. sativa* subsp. *indica*, WRC17), RGA4 (*O. sativa* subsp. *japonica*, Sasanishiki), RGA4-Oru (*O. rufipogon* accession W1943), RGA4-Oau (*O. australiensis* accession W0008), and RGA4-Ogr (*O. granulata* accession W0067B) (pCambia1300S-"helper NLR":HA), were generated by PCR amplification of the coding sequences from cDNA generated from leaf material and cloned into the binary vector pCambia1300S (www.cambia.org) that had been linearized by digestion with *Pst*I and *Spe*I by In-Fusion cloning. Expression constructs for two types of sensor NLRs, Pias-2 (*O. sativa* subsp. *indica*, WRC17) and RGA5 (*O. sativa* subsp. *japonica*, Sasanishiki) (pCambia1300S-FLAG: "sensor NLR"), were generated by PCR amplification of the coding sequences from cDNA generated from leaf material and cloned into the binary vector pCambia1300S (www.cambia.org) that had been linearized by digestion with *Sal*I and *Pst*I by In-Fusion cloning. The resulting vectors were introduced into *A. tumefaciens* (strain GV3101). The primers used to generate the expression constructs are listed in Dataset S5.

Cell-Death Assay in *N. benthamiana*. Transient expression of Pias/Pia allelic NLR and AVR-Pia was performed by infiltrating 4- to 5-wk-old *N. benthamiana* plants with *A. tumefaciens* carrying the expression vector. *A. tumefaciens* suspensions in infiltration buffer (10 mM 2-[*N*-morpholino]ethanesulfonic acid), 10 mM $MgCl_2$, and 150 μM acetosyringone, pH 5.6) were adjusted to the densities shown in *SI Appendix*, Table S7. The autofluorescence value under ultraviolet (UV) light was scored using a luminescent image analyzer (ImageQuant LAS-4000, Cytiva).

Data Availability. The DNA-seq and RNA-seq data from this study are listed in Dataset S6 and have been deposited in the DNA Databank of Japan (BioProject accession nos. PRJDB9440, PRJDB12353, PRJDB12884, PRJDB12891, and PRJDB12902). The nucleotide sequences of *Pias-1*, *Pias-2*, and *AVR-Pias* have been deposited in the DNA Databank of Japan (*Pias-1*: LC672059; *Pias-2*: LC672060; and *AVR-Pias*: LC672061).

All study data are included in the article and/or supporting information.

ACKNOWLEDGMENTS. This study was supported by Japan Society for the Promotion of Science KAKENHI 15H05779, 20H05681, and 16H06279 (PAGS) (to R.T.) and 21K14834 (to M.S.), Royal Society UK–Japan International Exchange Grants JPJSBP120215702 and IEC\R3\203081 (to R.T., S.K., and M.J.B.), the Biotechnology and Biological Sciences Research Council (UKRI-BBSRC, UK Grant BB/P012574), European Research Council (ERC BLASTOFF Project 743165), John Innes Foundation, and Gatsby Charitable Foundation. Computations were partially performed on the supercomputer at the Research Organization of Information and Systems, National Institute of Genetics. We also thank the National Institute of Genetics (National BioResource Project), Japan, and the Genebank at the National Agriculture and Food Research Organization, Japan, for providing the seeds of wild rice and WRC17, respectively.

Author affiliations: [a]Iwate Biotechnology Research Center, Kitakami, Iwate 024-0003, Japan; [b]Laboratory of Crop Evolution, Graduate School of Agriculture, Kyoto University, Mozume, Muko, Kyoto 617-0001, Japan; [c]Institute of Agrobiological Sciences, National Agriculture and Food Research Organization, Tsukuba, Ibaraki 305-8602, Japan; [d]Department of Molecular Microbiology, Tokyo University of Agriculture, Setagaya-ku, Tokyo 156-8502, Japan; [e]The Sainsbury Laboratory, University of East Anglia, Norwich NR4 7UH, United Kingdom; and [f]Department of Biochemistry and Metabolism, John Innes Centre, Norwich NR4 7UH, United Kingdom

1. S. A. Hogenhout, R. A. Van der Hoorn, R. Terauchi, S. Kamoun, Emerging concepts in effector biology of plant-associated organisms. *Mol. Plant Microbe Interact.* **22**, 115–122 (2009).
2. J. D. Jones, J. L. Dangl, The plant immune system. *Nature* **444**, 323–329 (2006).
3. J. Kourelis, R. A. L. van der Hoorn, Defended to the nines: 25 years of resistance gene cloning identifies nine mechanisms for R protein function. *Plant Cell* **30**, 285–299 (2018).
4. H. Adachi, L. Derevnina, S. Kamoun, NLR singletons, pairs, and networks: Evolution, assembly, and regulation of the intracellular immunoreceptor circuitry of plants. *Curr. Opin. Plant Biol.* **50**, 121–131 (2019).
5. R. M. Clark *et al.*, Common sequence polymorphisms shaping genetic diversity in *Arabidopsis thaliana*. *Science* **317**, 338–342 (2007).
6. A. L. Van de Weyer *et al.*, A species-wide inventory of NLR genes and alleles in *Arabidopsis thaliana*. *Cell* **178**, 1260–1272.e14 (2019).
7. Q. Pan, J. Wendel, R. Fluhr, Divergent evolution of plant NBS-LRR resistance gene homologues in dicot and cereal genomes. *J. Mol. Evol.* **50**, 203–213 (2000).
8. P. F. Sarris, V. Cevik, G. Dagdas, J. D. Jones, K. V. Krasileva, Comparative analysis of plant immune receptor architectures uncovers host proteins likely targeted by pathogens. *BMC Biol.* **14**, 8 (2016).
9. M. Bernoux *et al.*, Comparative analysis of the flax immune receptors L6 and L7 suggests an equilibrium-based switch activation model. *Plant Cell* **28**, 146–159 (2016).
10. J. Wang *et al.*, Ligand-triggered allosteric ADP release primes a plant NLR complex. *Science* **364**, eaav5868 (2019).

11. S. Ma *et al.*, Direct pathogen-induced assembly of an NLR immune receptor complex to form a holoenzyme. *Science* **370**, eabe3069 (2020).
12. R. Martin *et al.*, Structure of the activated ROQ1 resistosome directly recognizing the pathogen effector XopQ. *Science* **370**, eabd9993 (2020).
13. H. Sharif *et al.*, Structural mechanism for NEK7-licensed activation of NLRP3 inflammasome. *Nature* **570**, 338–343 (2019).
14. J. L. Tenthorey *et al.*, The structural basis of flagellin detection by NAIP5: A strategy to limit pathogen immune evasion. *Science* **358**, 888–893 (2017).
15. J. Wang *et al.*, Reconstitution and structure of a plant NLR resistosome conferring immunity. *Science* **364**, eaav5870 (2019).
16. L. Zhang *et al.*, Cryo-EM structure of the activated NAIP2-NLRC4 inflammasome reveals nucleated polymerization. *Science* **350**, 404–409 (2015).
17. G. Bi *et al.*, The ZAR1 resistosome is a calcium-permeable channel triggering plant immune signaling. *Cell* **184**, 3528–3541.e12 (2021).
18. L. Wan *et al.*, TIR domains of plant immune receptors are NAD^+-cleaving enzymes that promote cell death. *Science* **365**, 799–803 (2019).
19. S. Horsefield *et al.*, NAD^+ cleavage activity by animal and plant TIR domains in cell death pathways. *Science* **365**, 793–799 (2019).
20. H. Adachi, S. Kamoun, A. Maqbool, A resistosome-activated 'death switch.' *Nat. Plants* **5**, 457–458 (2019).
21. K. V. Krasileva, D. Dahlbeck, B. J. Staskawicz, Activation of an *Arabidopsis* resistance protein is specified by the in planta association of its leucine-rich repeat domain with the cognate oomycete effector. *Plant Cell* **22**, 2444–2458 (2010).
22. T. Kroj, E. Chanclud, C. Michel-Romiti, X. Grand, J. B. Morel, Integration of decoy domains derived from protein targets of pathogen effectors into plant immune receptors is widespread. *New Phytol.* **210**, 618–626 (2016).
23. S. J. Williams *et al.*, Structural basis for assembly and function of a heterodimeric plant immune receptor. *Science* **344**, 299–303 (2014).
24. C. Le Roux *et al.*, A receptor pair with an integrated decoy converts pathogen disabling of transcription factors to immunity. *Cell* **161**, 1074–1088 (2015).
25. Y. Okuyama *et al.*, A multifaceted genomics approach allows the isolation of the rice *Pia*-blast resistance gene consisting of two adjacent NBS-LRR protein genes. *Plant J.* **66**, 467–479 (2011).
26. S. Cesari *et al.*, The rice resistance protein pair RGA4/RGA5 recognizes the *Magnaporthe oryzae* effectors AVR-Pia and AVR1-CO39 by direct binding. *Plant Cell* **25**, 1463–1481 (2013).
27. I. Ashikawa *et al.*, Two adjacent nucleotide-binding site-leucine-rich repeat class genes are required to confer *Pikm*-specific rice blast resistance. *Genetics* **180**, 2267–2276 (2008).
28. A. Maqbool *et al.*, Structural basis of pathogen recognition by an integrated HMA domain in a plant NLR immune receptor. *eLife* **4**, e08709 (2015).
29. H. Takagi *et al.*, MutMap-Gap: Whole-genome resequencing of mutant F2 progeny bulk combined with de novo assembly of gap regions identifies the rice blast resistance gene *Pii*. *New Phytol.* **200**, 276–283 (2013).
30. K. Fujisaki *et al.*, An unconventional NOI/RIN4 domain of a rice NLR protein binds host EXO70 protein to confer fungal immunity. bioRxiv [Preprint] (2017). https://www.biorxiv.org/content/10.1101/239400v1 (Accessed 24 December 2017).
31. C. H. Wu *et al.*, NLR network mediates immunity to diverse plant pathogens. *Proc. Natl. Acad. Sci. U.S.A.* **114**, 8113–8118 (2017).
32. P. C. Bailey *et al.*, Dominant integration locus drives continuous diversification of plant immune receptors with exogenous domain fusions. *Genome Biol.* **19**, 23 (2018).
33. E. Pennisi, Armed and dangerous. *Science* **327**, 804–805 (2010).
34. J. Liu *et al.*, Recent progress and understanding of the molecular mechanisms of the rice-*Magnaporthe oryzae* interaction. *Mol. Plant Pathol.* **11**, 419–427 (2010).
35. Y. Wu *et al.*, Combination patterns of major R genes determine the level of resistance to the *M. oryzae* in rice (*Oryza sativa* L.). *PLoS One* **10**, e0126130 (2015).
36. M. J. Orbach, L. Farrall, J. A. Sweigard, F. G. Chumley, B. Valent, A telomeric avirulence gene determines efficacy for the rice blast resistance gene *Pi-ta*. *Plant Cell* **12**, 2019–2032 (2000).
37. Y. Jia, S. A. McAdams, G. T. Bryan, H. P. Hershey, B. Valent, Direct interaction of resistance gene and avirulence gene products confers rice blast resistance. *EMBO J.* **19**, 4004–4014 (2000).
38. H. Kanzaki *et al.*, Arms race co-evolution of *Magnaporthe oryzae AVR-Pik* and rice *Pik* genes driven by their physical interactions. *Plant J.* **72**, 894–907 (2012).
39. K. Fujisaki *et al.*, Rice Exo70 interacts with a fungal effector, AVR-Pii, and is required for AVR-Pii-triggered immunity. *Plant J.* **83**, 875–887 (2015).
40. C. H. Park *et al.*, The E3 ligase APIP10 connects the effector AvrPiz-t to the NLR receptor Piz-t in rice. *PLoS Pathog.* **12**, e1005529 (2016).
41. R. Wang *et al.*, Immunity to rice blast disease by suppression of effector-triggered necrosis. *Curr. Biol.* **26**, 2399–2411 (2016).
42. R. Zdrzałek, S. Kamoun, R. Terauchi, H. Saitoh, M. J. Banfield, The rice NLR pair Pikp-1/Pikp-2 initiates cell death through receptor cooperation rather than negative regulation. *PLoS One* **15**, e0238616 (2020).
43. Y. Kojima, K. Ebana, S. Fukuoka, T. Nagamine, M. Kawase, Development of an RFLP-based rice diversity research set of germplasm. *Breed. Sci.* **55**, 431–440 (2005).
44. P. Li *et al.*, RGAugury: A pipeline for genome-wide prediction of resistance gene analogs (RGAs) in plants. *BMC Genomics* **17**, 852 (2016).
45. H. Zhao *et al.*, The rice blast resistance gene *Ptr* encodes an atypical protein required for broad-spectrum disease resistance. *Nat. Commun.* **9**, 2039 (2018).
46. X. Meng *et al.*, The broad-spectrum rice blast resistance (R) gene *Pita2* encodes a novel R protein unique from *Pita*. *Rice (N. Y.)* **13**, 19 (2020).
47. S. V. Edwards, P. W. Hedrick, Evolution and ecology of MHC molecules: From genomics to sexual selection. *Trends Ecol. Evol.* **13**, 305–311 (1998).
48. F. Tajima, Statistical method for testing the neutral mutation hypothesis by DNA polymorphism. *Genetics* **123**, 585–595 (1989).
49. S. Césari *et al.*, The NB-LRR proteins RGA4 and RGA5 interact functionally and physically to confer disease resistance. *EMBO J.* **33**, 1941–1959 (2014).
50. K. Yoshida *et al.*, Association genetics reveals three novel avirulence genes from the rice blast fungal pathogen *Magnaporthe oryzae*. *Plant Cell* **21**, 1573–1591 (2009).
51. K. Oikawa *et al.*, The blast pathogen effector AVR-Pik binds and stabilizes rice heavy metal-associated (HMA) proteins to co-opt their function in immunity. bioRxiv [Preprint] (2020). https://www.biorxiv.org/content/10.1101/2020.12.01.406389v1.full (Accessed 2 December 2020).
52. A. Białas *et al.*, Two NLR immune receptors acquired high-affinity binding to a fungal effector through convergent evolution of their integrated domain. *eLife* **10**, e66961 (2021).
53. J. H. R. Maidment *et al.*, Multiple variants of the fungal effector AVR-Pik bind the HMA domain of the rice protein OsHIPP19, providing a foundation to engineer plant defense. *J. Biol. Chem.* **296**, 100371 (2021).
54. F. Lv *et al.*, GhCFE1A, a dynamic linker between the ER network and actin cytoskeleton, plays an important role in cotton fibre cell initiation and elongation. *J. Exp. Bot.* **66**, 1877–1889 (2015).
55. W. Truman, M. H. Bennett, I. Kubigsteltig, C. Turnbull, M. Grant, *Arabidopsis* systemic immunity uses conserved defense signaling pathways and is mediated by jasmonates. *Proc. Natl. Acad. Sci. U.S.A.* **104**, 1075–1080 (2007).
56. Y. Zhang, F. Zhang, X. Huang, Characterization of an *Arabidopsis thaliana* DUF761-containing protein with a potential role in development and defense responses. *Theor. Exp. Plant Physiol.* **31**, 303–316 (2019).
57. N. Takahata, M. Nei, Allelic genealogy under overdominant and frequency-dependent selection and polymorphism of major histocompatibility complex loci. *Genetics* **124**, 967–978 (1990).
58. S. B. Piertney, M. K. Oliver, The evolutionary ecology of the major histocompatibility complex. *Heredity* **96**, 7–21 (2006).
59. M. E. Woolhouse, J. P. Webster, E. Domingo, B. Charlesworth, B. R. Levin, Biological and biomedical implications of the co-evolution of pathogens and their hosts. *Nat. Genet.* **32**, 569–577 (2002).
60. R. Terauchi, K. Yoshida, Towards population genomics of effector-effector target interactions. *New Phytol.* **187**, 929–939 (2010).
61. C. A. Schneider, W. S. Rasband, K. W. Eliceiri, NIH Image to ImageJ: 25 years of image analysis. *Nat. Methods* **9**, 671–675 (2012).
62. D. Miki, K. Shimamoto, Simple RNAi vectors for stable and transient suppression of gene function in rice. *Plant Cell Physiol.* **45**, 490–495 (2004).
63. M. Mikami, S. Toki, M. Endo, Comparison of CRISPR/Cas9 expression constructs for efficient targeted mutagenesis in rice. *Plant Mol. Biol.* **88**, 561–572 (2015).
64. J. Sweigard, F. Chumley, A. Carroll, L. Farrall, B. Valent, A series of vectors for fungal transformation. *Fungal Genet. Newsl.* **44**, 52–55 (1997).
65. T. Arazoe *et al.*, Tailor-made CRISPR/Cas system for highly efficient targeted gene replacement in the rice blast fungus. *Biotechnol. Bioeng.* **112**, 2543–2549 (2015).
66. M. Shimizu *et al.*, RNA-seq of in planta-expressed *Magnaporthe oryzae* genes identifies MoSVP as a highly expressed gene required for pathogenicity at the initial stage of infection. *Mol. Plant Pathol.* **20**, 1682–1695 (2019).
67. Q. Zhao *et al.*, Pan-genome analysis highlights the extent of genomic variation in cultivated and wild rice. *Nat. Genet.* **50**, 278–284 (2018).
68. H. Du *et al.*, Sequencing and de novo assembly of a near complete *indica* rice genome. *Nat. Commun.* **8**, 15324 (2017).
69. International Rice Genome Sequencing Project, The map-based sequence of the rice genome. *Nature* **436**, 793–800 (2005).
70. Z. Wu *et al.*, De novo genome assembly of *Oryza granulata* reveals rapid genome expansion and adaptive evolution. *Commun. Biol.* **1**, 84 (2018).
71. A. V. Zimin *et al.*, Hybrid assembly of the large and highly repetitive genome of *Aegilops tauschii*, a progenitor of bread wheat, with the MaSuRCA mega-reads algorithm. *Genome Res.* **27**, 787–792 (2017).
72. M. Mascher *et al.*, A chromosome conformation capture ordered sequence of the barley genome. *Nature* **544**, 427–433 (2017).
73. J. L. Bennetzen *et al.*, Reference genome sequence of the model plant *Setaria*. *Nat. Biotechnol.* **30**, 555–561 (2012).
74. A. V. Zimin *et al.*, The MaSuRCA genome assembler. *Bioinformatics* **29**, 2669–2677 (2013).
75. H. Li, R. Durbin, Fast and accurate long-read alignment with Burrows-Wheeler transform. *Bioinformatics* **26**, 589–595 (2010).
76. A. Löytynoja, N. Goldman, webPRANK: A phylogeny-aware multiple sequence aligner with interactive alignment browser. *BMC Bioinformatics* **11**, 579 (2010).
77. B. Q. Minh *et al.*, IQ-TREE 2: New models and efficient methods for phylogenetic inference in the genomic era. *Mol. Biol. Evol.* **37**, 1530–1534 (2020).
78. D. T. Hoang, O. Chernomor, A. von Haeseler, B. Q. Minh, L. S. Vinh, UFBoot2: Improving the ultrafast bootstrap approximation. *Mol. Biol. Evol.* **35**, 518–522 (2018).
79. S. Kalyaanamoorthy, B. Q. Minh, T. K. F. Wong, A. von Haeseler, L. S. Jermiin, ModelFinder: Fast model selection for accurate phylogenetic estimates. *Nat. Methods* **14**, 587–589 (2017).
80. V. Ranwez, E. J. P. Douzery, C. Cambon, N. Chantret, F. Delsuc, MACSE v2: Toolkit for the alignment of coding sequences accounting for frameshifts and stop codons. *Mol. Biol. Evol.* **35**, 2582–2584 (2018).
81. S. Kumar, G. Stecher, M. Li, C. Knyaz, K. Tamura, MEGA X: Molecular evolutionary genetics analysis across computing platforms. *Mol. Biol. Evol.* **35**, 1547–1549 (2018).
82. Z. Yang, R. Nielsen, Estimating synonymous and nonsynonymous substitution rates under realistic evolutionary models. *Mol. Biol. Evol.* **17**, 32–43 (2000).
83. Z. Yang, PAML: A program package for phylogenetic analysis by maximum likelihood. *Comput. Appl. Biosci.* **13**, 555–556 (1997).